Computational Materials Science 237 (2024) 112916

Contents lists available at ScienceDirect

Computational Materials Science

journal homepage: www.elsevier.com/locate/commatsci

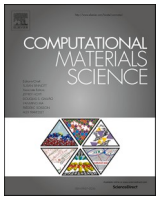

Full Length Article

Multiphysics modeling of frontal curing-enabled additive manufacturing for carbon fiber/thermoset composites

Weijia Yan [a], Ruochen Liu [b], Caleb Fowler [a], Shiren Wang [b], Jingjing Qiu [a,*]

[a] Department of Mechanical Engineering, Texas A&M University, College Station, TX 77843, USA
[b] Department of Industrial and Systems Engineering, Texas A&M University, College Station, TX 77843, USA

ARTICLE INFO

Keywords:
Advanced manufacturing
3D printing
Frontal curing
Epoxy

ABSTRACT

Frontal curing (FC) is an emerging self-sustainable exothermic reaction that attracts increasing attention. Such a technique provides a rapid and energy-efficient way for thermosets and their fiber composites to be in-situ printed and simultaneously cured using additive manufacturing (AM) methods. In this study, finite element analysis (FEA) was used to simulate FC-enabled additive manufacturing (FCAM) of thermosetting epoxy resin and its composites consisting of continuous or discontinuous carbon fiber (cCF/dCF). A curing reaction model and a thermal diffusion model were integrated to simulate FCAM of carbon fiber/epoxy composites with diverse 3D geometries. This study outlines the crucial factors for FCAM and clarifies how the frontal velocity, frontal temperature, and degree of cure in FCAM are influenced by different material compositions and various reaction kinetic parameters. The FEA results show that 20 wt% cCF/epoxy composites with an activation energy of 60 KJ/mol exhibit a frontal velocity of 4.3 cm/min and a frontal temperature of 288 °C during the continuous FCAM process, which are consistent with the experimental results. Case studies on a self-supportive spiral structure and a 6-meter wind blade tip were carried out to provide a guideline on material design and process control for scalable FCAM of 3D complex geometries.

1. Introduction

Advanced manufacturing (AM) of thermosets has emerged as a prominent technology to fabricate high-performance thermosets with 3D complicated geometries and controllable material characteristics such as porosity and microstructure. Nevertheless, most current AM technologies generally require high energy input, such as laser powder bed fusion (PBF), vat photopolymerization (VP), and direct energy deposition (DED), etc. Furthermore, following those 3D printing processes, thermoset composite products are typically required to undergo a subsequent cleaning process (i.e., to remove the sacrificial materials) or a post-curing treatment for a complete crosslinking. In recent years, frontal curing (FC, or called frontal polymerization), a heat-initiated spontaneous exothermic reaction, has attracted increasing attention by offering an energy-efficient AM method with in-situ curing capability. Frontal curing was first proposed in 1972 [1] but was not integrated with direct ink writing (DIW) until the first attempt to utilize frontal ring-opening metathesis polymerization for the self-curing of dicyclopentadiene (DCPD) in the DIW process [2]. This FC-enabled AM (FCAM) process differs from conventional thermosetting 3D printing processes by the curing initiation with a transient energy supply (for only several seconds before removal) without requiring synchronized thermal heating or optical heating through the entire printing process. After initiation, the exothermic curing reaction is quickly propagated to the neighboring regions and proceeds until the whole part is cured. The curing reaction is fast, and the energy cost is reduced by several orders of magnitude compared to conventional curing methods. In FCAM processes, FC generates self-sustaining reaction heat in thermosetting filaments immediately after filament deposition, making high-temperature curing more energy- and time-efficient. FCAM has demonstrated advantages for in-air printing of free-standing 3D complex thermosetting parts with mechanical properties comparable to those fabricated by traditional autoclave or oven curing techniques [3–5]. However, it is still challenging to achieve a controllable reaction rate or to maintain an appropriate curing temperature through a continuous FC-enabled DIW process, particularly for large thermosetting components.

Among diverse thermosetting polymers, Epoxy stands out with processing simplicity, high mechanical strength, excellent adhesion, good electrical insulating properties, as well as superior resistance to heat, chemicals, and corrosion [6]. Epoxy demonstrates a wide range of

* Corresponding author.
E-mail address: jennyqiu@tamu.edu (J. Qiu).

https://doi.org/10.1016/j.commatsci.2024.112916
Received 20 December 2023; Received in revised form 22 February 2024; Accepted 24 February 2024
Available online 29 February 2024

applications in aerospace, marine, automotive, construction, and sporting equipment [7]. Epoxy polymer and its composites are among the most explored materials in FC thus far [8–11]. The addition of nanoparticles, such as modified carbon nanotubes (CNTs), further improved the impact resistance and environmental stress-cracking resistance of CNTs/epoxy nanocomposites. Akram et al. have developed epoxy nanocomposites using polyacrylonitrile/multi-walled CNTs and polyacrylonitrile/carbon nanofiber aerogel scaffolds [12]. The high tensile strength, lightweight, and excellent durability of continuous carbon fibers or glass fibers also contributed to improved mechanical performance of the epoxy-based composites. Anh et. al also fabricated fiber reinforced epoxy composites with up to 74 vol% of glass microspheres and 40 vol% of short carbon fibers by using radical induced cationic frontal polymerization. These epoxy composites indicated similar tensile strength compared to those cured using traditional thermal curing techniques [13]. In recent years, FC has been utilized for energy-efficient and fast printing of thermosets and their composites [14,15]. In this additive manufacturing process of thermoset parts, FC operates by mixing a resin with a latent initiator, which catalyzes the curing reaction of resins upon reaching the initiation temperatures. This localized curing generates heat that subsequently activates the initiator in proximate resin regions, creating a cascading "cure front" that propagates through the material. The focus of this epoxy printing process is to ensure that the material polymerizes efficiently as it exits the extrusion nozzle by initiating the curing reaction and extruding the material at a flow rate that matches the curing front velocity [4]. Recently, Zhang et al. developed FC-enabled in-situ printing and synchronized curing of continuous carbon fiber/epoxy thermoset composites with exceptional mechanical properties and low energy consumption. As-printed thermoset products demonstrate comparable mechanical performance as those fabricated by traditional curing techniques [16–18]. In this process, many factors including the choice of monomer, initiator/catalyst, additives, and fillers all play a critical role on the success of FC and further determine the frontal propagation velocity and maximal frontal temperature for synchronized printing and curing. However, there is still a lack of fundamental understanding of appropriate material composition, polymer chemistry, and proper print speed for an optimal reaction rate and an appropriate frontal temperature. Therefore, there remains an urgent need to develop numerical modeling of epoxy FCAM to identify optimal material compositions and printing parameters.

At present, there have been multiple mathematical models introduced to describe frontal polymerization in a variety of chemicals [2,19–21]. In the recent publications on FCAM, finite element analysis (FEA) was employed to simulate and evaluate the impact of different factors on the in-situ FC effects [22–24]. Goli et al. developed an FEA-based numerical model to study the initiation and propagation of a polymerization front in dicyclopentadiene (DCPD). The role of heat diffusion on the appearance of instabilities was investigated during the frontal polymerization of an adiabatic channel of neat DCPD resin and of unidirectional carbon fiber/DCPD composites based on a thermo-chemical reaction–diffusion model [25–27]. Based on this research, Vyas et al. found that the maximum frontal temperature of glass fiber/DCPD composites was comparable to that of carbon fiber/DCPD composites [28]. Compared to DCPD, epoxy and its composites cover ~ 70 % of the thermosetting resin market [29] due to its advantages in mechanical performance and durability [6]. Frulloni et al. used a finite difference method to simulate the front polymerization process for an epoxy–amine thermoset system [30]. Recently, Wang et al. examined the effect of the microstructures on the frontal polymerization of unidirectional carbon fiber/epoxy composites using FEA [31]. It was found that FEA simulation can provide critical guidelines on rational material composition design and optimal process control to ensure a successful implementation of FCAM.

In this work, FEA is used for numerical modeling of FCAM process for an innovative self-curable epoxy system as a function of different material compositions and various reaction kinetic parameters. The effects of activation energy and enthalpy of curing reaction on the curing frontal propagation are studied numerically by controlling material compositions, such as fiber composition/ volume fractions. The FEM simulations in this study focus on the spontaneous and continuous FC-enabled 3D printing process of a specified epoxy monomer-initiator system, with or without the incorporation of fiber reinforcement. The reaction kinetic parameters and other material property data are obtained from experimental measurements. The spatio-temporal evolution of frontal velocity and frontal temperature are evaluated for optimal curing effects and proper printing speeds.

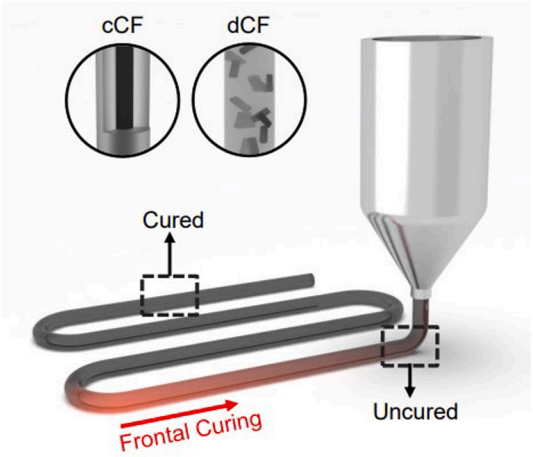

Fig. 1. The principle of FCAM printing of fiber-reinforced thermosetting composites.

2. Methods

2.1. The process for FCAM

As illustrated in Fig. 1, a FCAM process developed by our research group was studied [32]. In this method, frontal curing of carbon fibers (CF)/epoxy composites was tuned by synchronizing self-sustaining frontal propagation rate and printing process, as shown in Fig. 1. Different geometric structures can be demonstrated by this FCAM process. Instantaneous curing right after extrusion allowes the printed structure to retain its form, enabling in-situ curing into 3D free-standing shapes such as spiral structures and gyroid structures, which are difficult to construct in conventional additive manufacturing without using supporting materials. In this paper, FEA was used to simulate this FCAM process to ensure continuous printing/in-situ curing for high-performance CF/epoxy composites and thus to reduce the trial-and-error efforts in the experiments.

2.2. Governing equation

The thermal conduction and curing reaction kinetics associated with this FCAM process can be described as a coupled reaction–diffusion model:

$$k(\nabla\cdot\nabla T)+\rho H_r\frac{\partial a}{\partial t}=\rho C_p\frac{\partial T}{\partial t} \tag{1}$$

$$\frac{\partial\alpha}{\partial t}=A\cdot\exp\left(-\frac{E_a}{RT}\right)\cdot(1-\alpha)^n\cdot(\alpha)^m\cdot\frac{1}{1+\exp(C(\alpha-\alpha_c))} \tag{2}$$

The first equation is a diffusion equation that governs heat transfer in epoxy with a source term characterized by the enthalpy of the reaction H_r [J/kg], which denotes the heat generation from the chemical reaction. The second equation is the curing kinetic equation used to describe

the degree of cure α [non-dimensional] and the curing rate $\frac{\partial \alpha}{\partial t}$ [/s] as a function of temperature [K]. The terms k [W/(m·K)], ρ [kg/m^3], and C_p [J/(kg·K)] denote the thermal conductivity, density, and heat capacity of the printing ink, respectively. The first term of the diffusion equation (1), $k(\nabla \cdot \nabla T)$, represents the heat conduction from adjacent sections of material. The second term, $\rho H_r \frac{\partial \alpha}{\partial t}$, represents the heat generated by curing. The third part, $\rho C_p \frac{\partial T}{\partial t}$, is the rate of change of energy in the material.

The front propagation velocity and maximal frontal temperature will be derived in the Cartesian coordinate system for either continuous carbon fiber (cCF)/epoxy composites or discontinuous carbon fibers (dCFs)/epoxy composites. In the first term of equation (1), the heat conductivity of composites is estimated by the rule of mixture. Further, the thermal conductivity of carbon fibers was considered as anisotropic with a greater value along the axial direction of fiber tows [32,33]. It is assumed that the thermal conductivity for dCF is isotropic considering randomized fiber distribution. The second term is calculated by the product of the resin volume fraction and the resin density. The heat capacity in the third term is also estimated by the rule of mixture.

The curing kinetics equation (2) describing the curing process that a resin is governed by the Prout-Tompkins model for autoactivation effects with a diffusion term. In this equation, A [1/s] is the rate constant, E_a [KJ/mol] is the activation energy, R [8.314 J/(mol·K)] is the universal gas constant, n and m are the reaction order constants in the Prout-Tompkins model [34]. C is the diffusion domination coefficient and α_c is the diffusion domination threshold. In this work, $\frac{1}{1+exp(C(\alpha-\alpha_c))}$ is used to refine the reaction kinetics model when the curing kinetics are dominated by diffusion. This model was selected as the most complex and well-developed kinetic model for FC chemistry, which has been used in FC modeling of neat resin and composites [5,35,36]. The epoxy's degree of cure was initialized to 0 at t = 0 [5] and the diffusion domination threshold was set to 0.9 [25].

Moreover, the initial and boundary conditions of the current problem are:

$$T|_{t=0} = T_{amb} \tag{3}$$

$$T|_{x=0,0\le t\le t_{init}} = T_{init} \tag{4}$$

$$\alpha|_{t=0} = \alpha_0 \tag{5}$$

$$\frac{\partial T}{\partial x}|_{x=0,t>t_{init}} = 0 \tag{6}$$

Where all material temperatures were initialized to be ambient temperature T_{amb} at t = 0; T_{init} is the initiation temperature applied on the end of the as-printed filament. Heated surfaces were constrained to an initiation temperature during the initiation phase for seconds and simulated as normal after that. Heat conduction and convection are represented directly by heat fluxes according to Newton's law of cooling. Surface radiation is governed by the Stefan-Boltzmann law.

3. Results and discussion

3.1. Model implementation

In this work, the material properties, including reaction kinetic parameters, were integrated into the above governing diffusion–reaction model while returning the frontal velocity and the frontal temperature as output using COMSOL Multiphysics. In particular, the curing kinetics parameters, including the activation energy, enthalpy of reaction, and rate constant were discussed. FCAM was also applied in printing epoxy/fiber components with different geometries to explore the potential of FPAM in scaled-up manufacturing.

All the numerical solutions were cumulatively derived from multiple runs of simulations. The average values were summarized for comparison. Some simulation results for a representative cylindrical filament with a diameter of 1 mm and a length of 1.5 × 10^{-2} m are shown in Fig. 2. The spatiotemporal profiles for the frontal temperature were illustrated. In the case of the dCF/epoxy composite, it is assumed that the dCF is uniformly dispersed within the epoxy resin. For the cCF/epoxy composite, it is hypothesized that the carbon fibers are centrally positioned within the epoxy resin, as depicted in Fig. 2(c). Fig. 2(a) shows the frontal propagation of neat epoxy after 20 s of initiation at 230 °C. After initiation, a maximal frontal temperature of 245.04 °C, a frontal velocity of 1.2 cm/min, and a final conversion of 96.45 % were achieved. Fig. 2(b) indicates the frontal propagation in a dCF-epoxy composite. The rule of mixture was used to estimate the thermal conductivity, density, and heat capacity of the dCF-epoxy composite with a fiber weight percentage of 20 %. Our FEA simulation indicates a reduced frontal temperature of 228.78 °C, a frontal velocity of 2.4 cm/min, and a final conversion of 96.41 %. Fig. 2(c) indicates a representative geometry of the (cCF core/epoxy shell) filament. With the addition of 20 wt% cCFs, the frontal temperature decreases to 288.5 °C, the frontal velocity increases to 4.3 cm/min, and the final conversion also increases to 98.72 %.

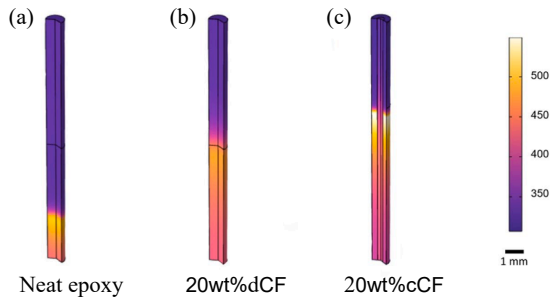

Fig. 2. Temperature distribution (K) after 20 s of initiation in (a) neat epoxy; (b) in 20 wt% dCF-epoxy composite (c) in 20 wt% cCF-epoxy composite.

Table 1
Frontal printing simulation results in neat epoxy, 20 wt% dCF, and 20 wt% cCF.

	Neat Epoxy	20 wt% dCF	20 wt% cCF
Frontal velocity (cm/min)	1.2	2.4	4.3
Frontal temperature (K)	518.19	501.93	561.65
Degree of Cure	0.9645	0.9641	0.9872

The frontal velocity is calculated by the quotient of the reaction propagation span and the duration. Due to the consistent material properties along the propagation path and the constant filament cross-section area, the front propagation proceeds at a constant frontal velocity for all the 3 cases. Table 1 indicates that the frontal velocity of dCF/epoxy composites and cCF/epoxy composites increased by ~ 100 % and ~ 258 % compared to that of pristine epoxy resin, respectively. In contrast, the maximal frontal temperature of dCF/epoxy composites decreased by ~ 6.6 % whilst that of cCF/epoxy composites increased by ~ 17.7 % compared to that of pristine epoxy resin, respectively. Furthermore, due to the rapid frontal propagation and higher maximal frontal temperature, the degree of cure of cCF/epoxy composites is slightly larger than both those of pristine neat epoxy and dCF/epoxy composites.

The temporal profiles of the localized temperature and degree of cure were identified at a point located at a height of 1 cm to the initiation point at the bottom and were plotted in Figs. 3 and 4, respectively. The input material parameters for the simulation are outlined in the Appendix. Fig. 3 indicates an abrupt rise of the localized temperature at a rate up to ~ 102 K/s, ~93 K/s, and 160 K/s for neat epoxy, dCF/epoxy composite, and cCF/epoxy composite, respectively. After the localized temperature reaches the maximal frontal temperature, it starts to cool down. Although cCF/epoxy composite indicates a steeper temperature

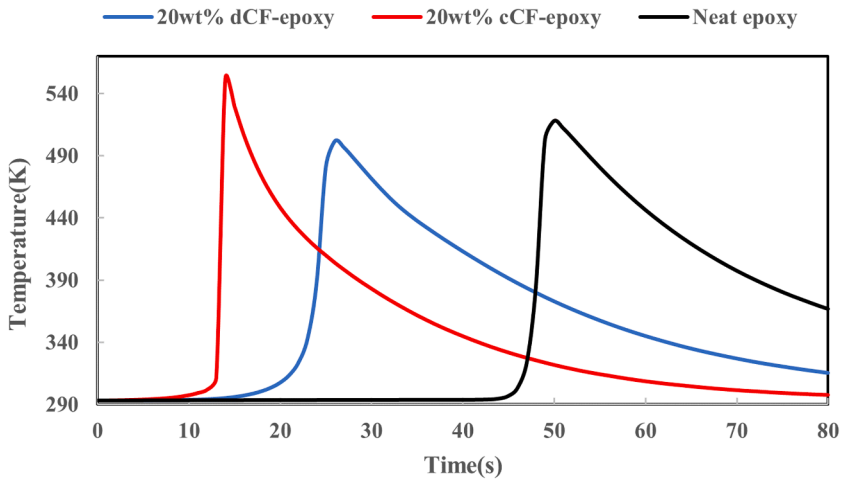

Fig. 3. Frontal temperature at a height of 1 cm to the initiation point for neat epoxy (black), 20 wt% dCF-epoxy composite (blue), and 20 wt% cCF-epoxy composite (red). (For interpretation of the references to colour in this figure legend, the reader is referred to the web version of this article.)

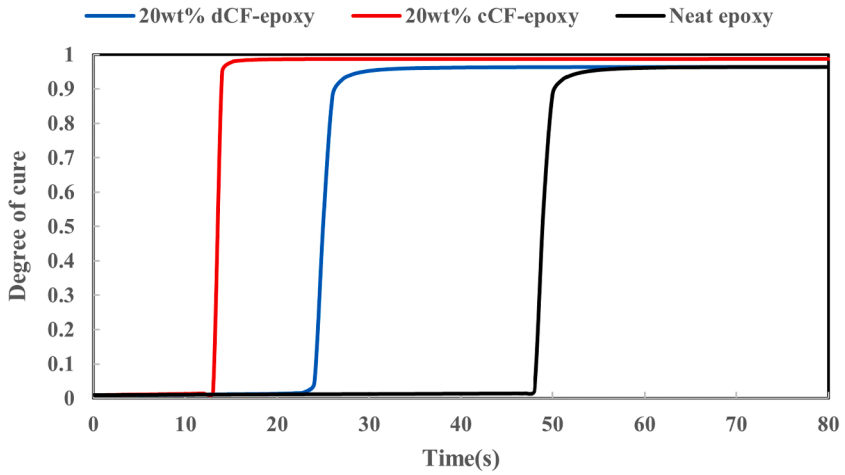

Fig. 4. Degree of cure at a height of 1 cm to the initiation point for neat epoxy (black), 20 wt% dCF-epoxy composite (blue), and 20 wt% cCF-epoxy composite (red). (For interpretation of the references to colour in this figure legend, the reader is referred to the web version of this article.)

Table 2
Frontal printing simulation results for cCF-epoxy composite with a fiber weight fraction ranging from 5 wt% to 40 wt%.

cCF weight fraction	5 %	10 %	15 %	20 %	25 %	30 %	35 %	40 %
Temperature (K)	546.0	550.5	552.1	561.6	574.9	575.1	575.4	578.5
Velocity (cm/min)	3.58	3.81	4.03	4.29	4.44	4.96	5.31	6.12
Degree of Cure	0.9885	0.9879	0.98739	0.98729	0.99116	0.9863	0.9828	0.9787

rise than both pure epoxy resin and dCF/epoxy composites, its maximal frontal temperature of 288.5 °C could result in thermal degradation of epoxy resin. In addition to the heat dissipation of epoxy shells in the printed filament, the higher thermal conductivity of cCF fiber cores also contributes to a quicker thermal conduction during the cooling process, resulting in a swifter temperature drop.

Fig. 4 indicates the simulation results of the degree of cure as a function of time, which represents the conversion percentage up to the point of complete curing. It was found that cCF/epoxy composite needs the least time to initiate curing and for a complete curing due to the higher thermal conductivity of cCFs. Therefore, the numerical modeling results indicate that the integration of cCFs is in favor of faster 3D printing. The data in Table 1 fits exponential regression models with a high degree of accuracy, indicated by R^2 values exceeding 0.99. This observation aligns with the mathematical relationships defined by the constants in the Prout-Tompkins equation, expressed in Eq. (1). Our study validates that the interplay of parameters in the Prout-Tompkins model is reflected in the effective application of FCAM, which is consistent with the results reported by Kumar et al. [35]. This FEA modeling provides a theoretical guidance to achieve optimal FC chemistries for a complete curing of epoxies (see Table 2).

The simulation results were further validated by experimental studies. Briefly, cCF/epoxy resin inks were printed, and then in-situ cured using this FCAM technique. The filament deposition speed was synchronized with the propagation velocity of the reaction front to ensure continuous freeform printing. A forward-looking infrared camera (FLIR A325sc) was installed to record the thermal images during the FCAM process. The frontal temperature profiles for 40 wt% cCF-epoxy composites are illustrated in Fig. 5. The frontal velocity is calculated by the propagation distance per unit time. In these experiments, the

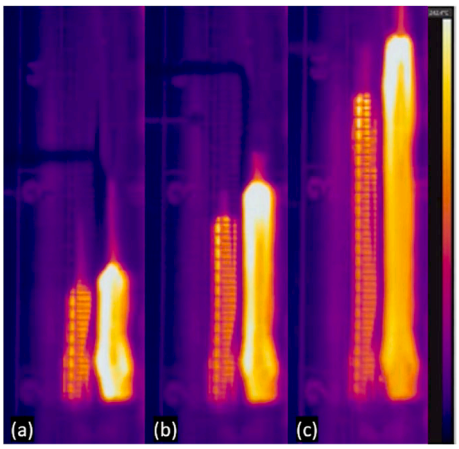

Fig. 5. Experimental results of FCAM and real-time IR image of 40 wt% cCF-epoxy composite after (a) 15 s, (b) 22 s, (c) 32 s.

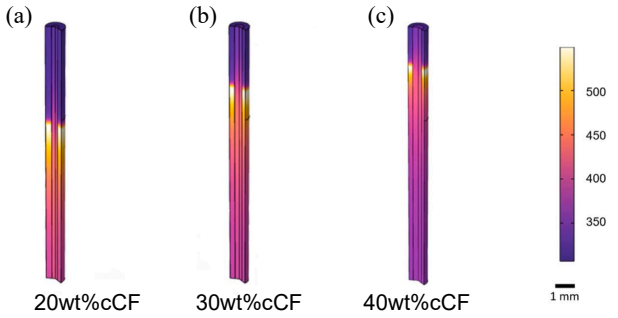

Fig. 6. Temperature distribution (K) after 20 s in (a) 20 wt%, (b) 30 wt%, and (c) 40 wt% cCF-epoxy composites.

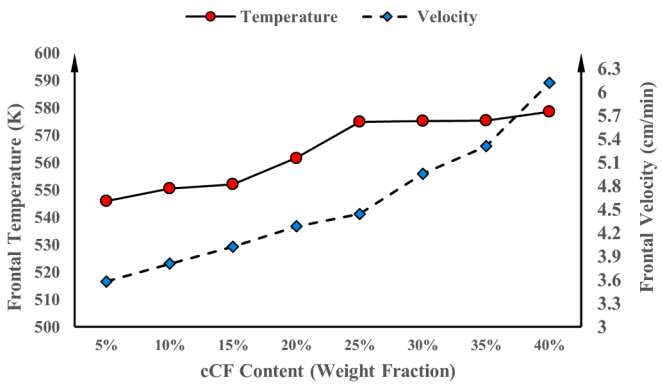

Fig. 7. Frontal temperature at a height of 1 cm to the initiation point for cCF-epoxy composites with a fiber weight percentage ranging from 5 wt% to 40 wt%.

frontal temperature was measured to range between 493 K and 563 K, which is consistent with the results reported in the literature[1617]. The simulation results listed in Table 2 align well with our experimental observations, as illustrated by Fig. 5.

The lower bound of FCAM performance can be estimated by the frontal characteristics from the threshold case. Variations in the process parameters and material properties could be tuned to indicate further increments in frontal temperature, propagation velocity, and degree of cure. High frontal temperatures are desirable to ensure a complete polymerization, but it is also possible to overheat epoxy during curing, a common problem during the fast propagation in FCAM. For a scaled-up

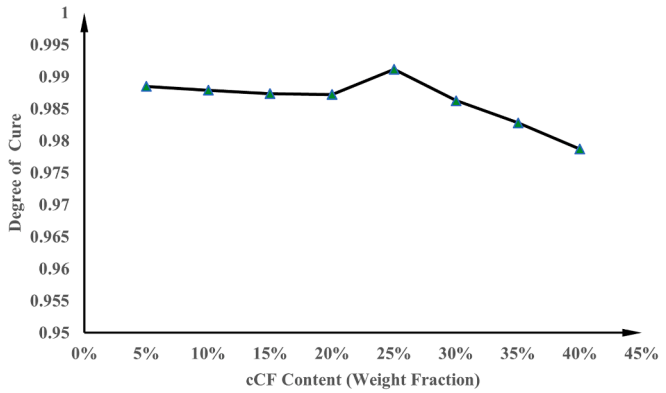

Fig. 8. Degree of cure at a height of 1 cm to the initiation point for cCF-epoxy composites with a fiber weight percentage ranging from 5 wt% to 40 wt%.

AM process, a higher frontal velocity is preferred to synchronize with the fast printing speed. Therefore, the material composition with a lower activation energy and the process parameters that offer large enthalpy of cure are desired to achieve fast printing and in-situ curing or epoxy resin.

3.2. *The effect of continuous carbon fiber weight percentage in FCAM*

In this task, the effect of cCF weight percentage on the requisite reaction kinetics was also studied. The spatiotemporal profiles of the curing front were simulated for various weight fractions of cCFs, as shown in Fig. 6. The range of cCF percentage to sustain continuous FCAM was determined, as shown in Fig. 7 and Fig. 8, respectively. The material parameters are outlined in the Appendix. The geometrical models of 1-mm diameter cCF core/epoxy resin shell filaments with different fiber core diameters were constructed. Specifically, for a fixed filament diameter, a higher cCF proportion results in a larger cCF core diameter and a thinner epoxy resin shell.

For 25 wt% cCF/epoxy composites, both the frontal temperature and degree of cure reach their peaks of 299 °C and 99.12 %, respectively. With a cCF content of above 25 wt%, there is no significant increment in the frontal temperature, while a slight reduction in the degree of cure is observed. This phenomenon can be attributed to two primary reasons. First, the incorporation of cCF enhances the frontal temperature, which might be close to the degradation temperature of epoxy, thereby setting a limit to a further temperature increment. Second, an excessive addition of carbon fibers leads to resin deficiency in the cCF/epoxy composite, resulting in an insufficient heat release to sustain either the frontal temperature or the degree of cure. This suggests that the impact of cCF content in cCF/epoxy composites is not simply linear. Therefore, in the experimental design of cCF/epoxy composites, an appropriate ratio of cCF to epoxy is essential to achieve continuous FCAM.

The effects of cCFs inclusion on the success of continuous FCAM provesses typically attributed to their elevated thermal conductivity and the additional heat capacity. In the case of low percentages of cCFs (below ~ 20 wt%), the frontal temperature of the epoxy sticking to the cCF core is slightly higher than the temperature in the epoxy shell region because cCFs are more thermally conductive along their length direction than the transverse direction. In comparison, the random orientation of dCFs results in the isotropic increment of the thermal conductivity in the dCFs/epoxy composite filaments. The frontal temperature is uniform along the transverse direction of those filaments. This is also consistent with our experimental results.

3.3. *The effect of activation energy for continuous carbon fiber reinforced epoxy in FCAM*

In this task, the effect of activation energy on the requisite reaction

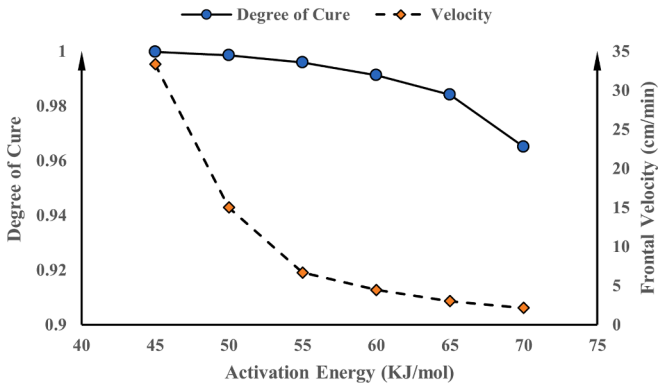

Fig. 9. Degree of cure and frontal velocity (cm/min) profiles for 25 wt% cCF-Epoxy composites as a function of activation energy E_a from 45 to 70 kJ/mol.

kinetics was also studied for cCF/epoxy composites. The spatiotemporal profiles of the curing front were simulated for various reaction kinetics of 25 wt% cCF/epoxy composites. The degree of cure, frontal velocity, and frontal temperature are shown in Fig. 9 and Fig. 10, respectively.

As shown in Table 3, the frontal temperature and frontal velocity were sampled for a range of activation energy from 45 KJ/mol to 70 KJ/mol, respectively. It was found that the frontal velocities vary from ~ 2.14-33.33 cm/min, as shown in Fig. 9. In contrast, the frontal temperatures exhibit less variability, ranging from ~ 267–300 °C, as shown in Fig. 10. Within this frontal temperature and frontal velocity range, the degree of cure varied slightly from 96.51 % to 99.98 %. This indicates that a lower activation energy of epoxy significantly results in a higher frontal velocity and a higher degree of cure in cCF-epoxy composites. Therefore, in practical FCAM applications, a lower activation energy close to 45 kJ/mol can facilitate a rapid production rate. For epoxy composites with an activation energy exceeding 70 kJ/mol, it is necessary to adjust other parameters to promote the occurrence of FCAM like increasing the reaction enthalpy or rate constant.

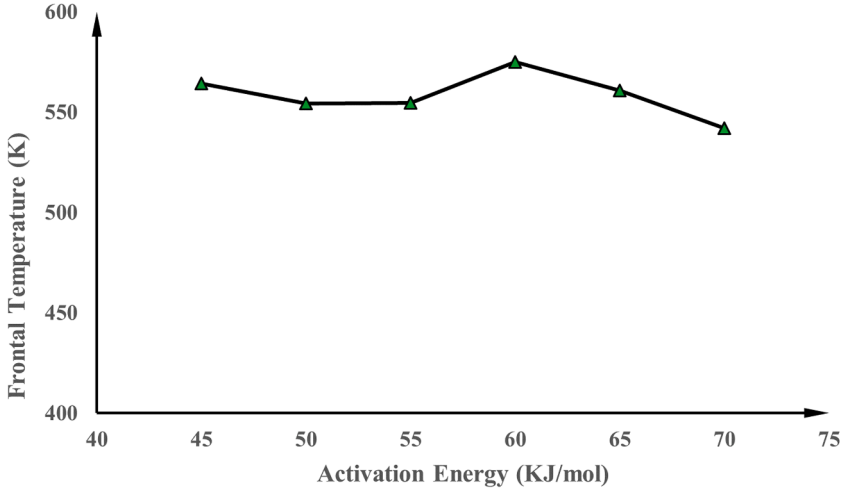

Fig. 10. Frontal temperature (K) profiles for 25 wt% cCF-Epoxy composites as a function of activation energy E_a from 45 to 70 kJ/mol.

Table 3
Frontal printing simulation results in 25 wt% cCF-Epoxy composites with different activation energy.

Activation Energy	45 kJ/mol	50 kJ/mol	55 kJ/mol	60 kJ/mol	65 kJ/mol	70 kJ/mol
Temperature (K)	564.27	554.6	554.46	574.91	560.62	541.94
Velocity (cm/s)	33.33	15	6.67	4.44	3	2.14
Degree of Cure	0.999765	0.998517	0.99583	0.991155	0.984153	0.96505

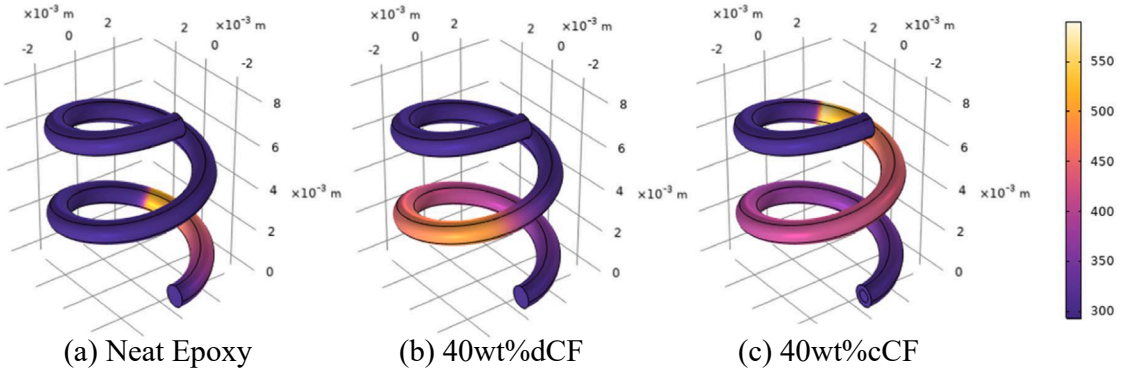

Fig. 11. Frontal temperature (K) profiles after 22 s for (a) neat epoxy, (b) 40 wt% dCFs/epoxy composite, and (c) 40 wt% cCFs/epoxy composite. Spiral structure geometry: a major radius of 3×10^{-3} m, a minor radius of 5×10^{-4} m, and a pitch of 4×10^{-3} m. Initiation at the bottom for 10 s.

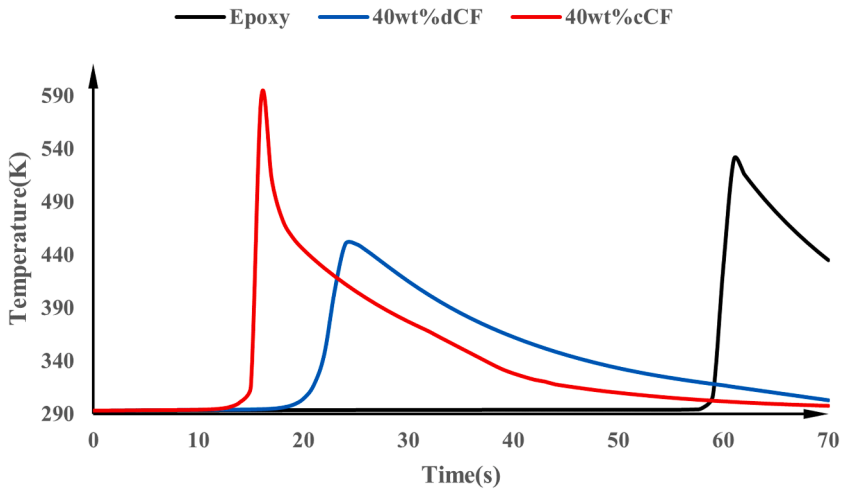

Fig. 12. Frontal temperature at a height of 0.4 cm to the initiation point for neat epoxy (black), 40 wt% dCF-epoxy composite (blue), and 40 wt% cCF-epoxy composites (red). (For interpretation of the references to colour in this figure legend, the reader is referred to the web version of this article.)

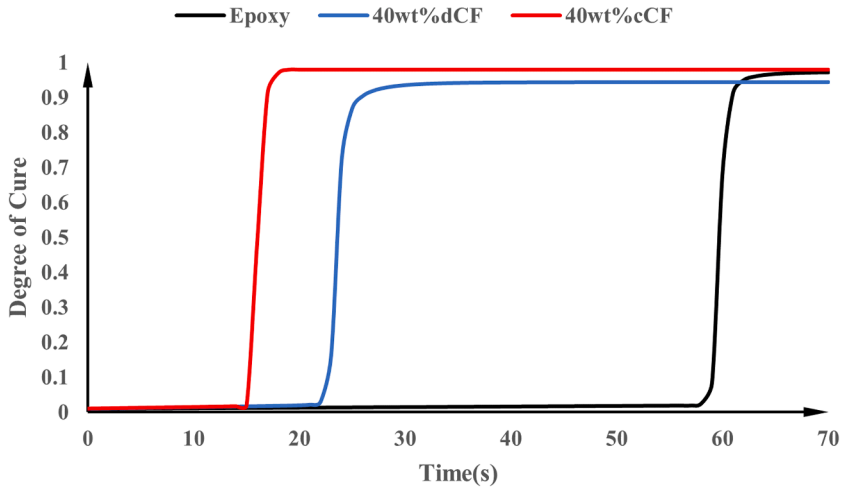

Fig. 13. Degree of cure for neat epoxy (black), 40 wt% dCFs/epoxy composite (blue), and 40 wt% dCFs/epoxy composites (red). (For interpretation of the references to colour in this figure legend, the reader is referred to the web version of this article.)

3.4. Case studies

An FCAM case study of spiral epoxy composites was investigated using COMSOL Multiphysics software, as shown in Fig. 11. Neat epoxy demonstrates a frontal temperature of 256 °C and a frontal velocity of 1.2 cm/min. A 40 wt% dCFs/epoxy composite indicates a frontal temperature of 180 °C and frontal velocity of 4.2 cm/min. A 40 wt% cCF/epoxy composite demonstrates a frontal temperature of 305 °C and frontal velocity of 6.1 cm/min.

The frontal temperature and the degree of cure for neat epoxy and CFs/epoxy composite are shown in Fig. 12 and Fig. 13, respectively. The frontal velocity for the 40 wt% dCFs/epoxy composite increases while the frontal temperature drops compared to those of pure epoxy. The degree of cure is also reduced slightly from 97.1 % to 94.4 % after the

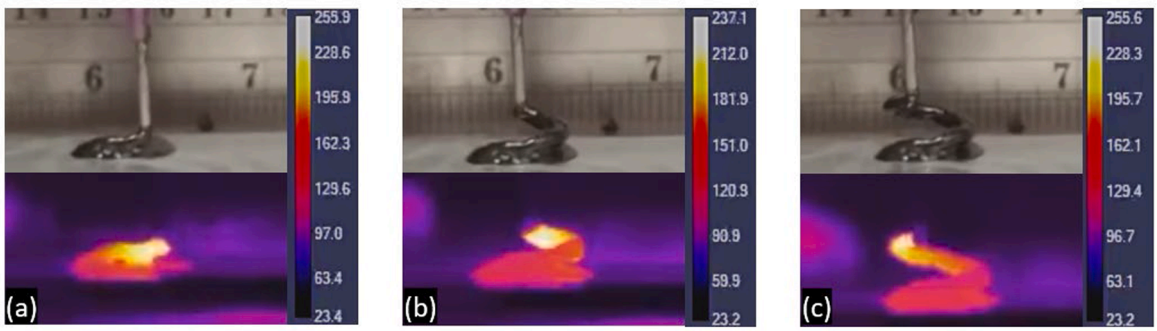

Fig. 14. Experimental results of FCAM and real-time IR image of 40 wt% cCF-epoxy composites after (a) 19 s, (b) 31 s, (c) 40 s.

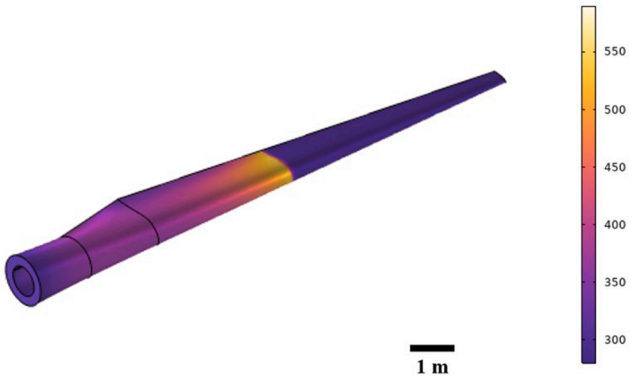

Fig. 15. Frontal temperature(K) profiles of a wind blade.

integration of 40 wt% dCFs. For the 40 wt% cCFs/epoxy composite, the frontal temperature increased about 19%, the frontal velocity increased about 5 folds, and the degree of cure is enhanced to 98.0 %. The conclusion is consistent with the previous trend observed with 20 wt% dCFs/epoxy and cCFs/epoxy composites, indicating that the introduction of both dCFs and cCFs can accelerate the frontal velocity. The introduction of dCFs reduces the frontal temperature, while the incorporation of cCFs increases it.

Furthermore, the simulation results were also verified through experimentation. As illustrated in Fig. 14, cCF core/resin shell filaments were deposited on a substrate for FCAM of free-standing spiral composites. The experiments indicated that an increment in the cCF content results in increased frontal temperature and frontal velocity. The presence of high thermal conductivity fiber bundles led to enhanced thermal diffusion along the propagation direction, significantly increasing the frontal velocity. For 40 wt% cCF-epoxy composites, the frontal velocity can be tuned up to $\sim$ 7 cm/min for continuous printing and synchronized in-situ curing. The experimental results demonstrate that the coupled FEA model is effective in predicting and analyzing the FCAM process for carbon fiber/epoxy composites within an acceptable margin of error. The minor differences between simulation and experimental results are mainly attributed to the uncertainties from the environmental conditions.

The FCAM process of a 6-meter 20 wt% dCF/epoxy composites wind blade was studied using FEA simulation, as shown in Fig. 15. The material parameters used in this model are also listed in the appendix. It is assumed that the dCF are uniformly distributed throughout the epoxy resin and the dCF/epoxy composites exhibit isotropic properties. The activation energy is 60 KJ/mol, the initiation temperature is 225 °C, initiation time is 10 s. In this case, the maximal frontal velocity of 40 wt % cCF/epoxy composites is about 4.1 folds compared to that of the neat epoxy. This simulation demonstrates the viability of FCAM in the manufacturing of large-scale components. The results provide a guideline for scalable FCAM of 3D complex geometries.

4. Conclusions

As an energy-efficient additive manufacturing technique, there is little work done quantitatively to model the (processing parameters)- and (material composition)-dependent frontal propagation in FCAM process of fibers reinforced epoxy composites. This paper indicates that the inclusion of carbon fiber for epoxy composites promotes a faster FCAM process of epoxy composites. Generally, both dCF and cCF additions enhance the frontal velocity, with cCF inclusion being more effective than dCF. With a specific activation energy of 60 KJ/mol, the maximum frontal velocity of the 40 wt% cCF-epoxy composites spiral component exceeds 6 cm/min, representing a 410 % increase compared to that of the neat epoxy. The integration of cCF raises both the frontal temperature and the degree of cure, while the incorporation of dCF slightly reduces the frontal temperature. In the case of cCF-epoxy composites, the impact of weight fractions with a range of 0 to 40 wt % and the activation energy between 45 and 70 KJ/mol on the FCAM process were investigated. It was found that larger proportions of cCF in the composites correlate with increased frontal velocity; however, changes in frontal temperature and degree of cure become less pronounced beyond 25 wt% due to the risks of epoxy decomposition and resin deficiency. Regarding activation energy, a lower activation energy contributes to a larger frontal velocity up to 33.3 cm/min. For an activation energy exceeding 70 KJ/mol, it might be necessary to adjust epoxy composition for an appropriate reaction enthalpy or rate constant to sustain a continuous FCAM. It is consistent with the experimental results[32]. The multiphysics simulation is effective in predicting the efficacy of FCAM for various material compositions and curing kinetics. This work provides valuable insights for the development of novel AM techniques of thermosetting composites, providing theoretical guidance on material design and manufacturing control of high-performance composites.

CRediT authorship contribution statement

Weijia Yan: Data curation, Formal analysis, Investigation, Formal analysis, Validation, Writing – original draft, Writing - review & editing. **Ruochen Liu:** Data curation, Investigation, Validation. **Caleb Fowler:** Data curation, Formal analysis, Writing - original draft. **Shiren Wang:** Funding Acquisition, Methodology, Resources, Software, Supervision, Validation. **Jingjing Qiu:** Conceptualization, Formal analysis, Funding Acquisition, Investigation, Methodology, Project administration, Resources, Supervision, Writing – review & editing.

Declaration of competing interest

The authors declare that they have no known competing financial interests or personal relationships that could have appeared to influence the work reported in this paper.

Data availability

Data will be made available on request.

Acknowledgment

This work is supported by the National Science Foundation (CMMI-1934120, CMMI-1933679, and CMMI-2310216).

Appendix

Table A1
Simulation parameters.

Parameter	Symbol (Unit)	Default	Range
Initiation			
Initial cure	α_{init}	0.01	–

(*continued on next page*)

Table A1 (*continued*)

Parameter	Symbol (Unit)	Default	Range
Heating time	$t_{init}(s)$	10	–
Heating Temperature	$T_{init}(K)$	500	–
Epoxy Properties			
Density	$\rho(kg/m^3)$	1160	–
Thermal Conductivity	$k(W/mK)$	0.2 [35]	–
Specific Heat	$C_p(J/kgK)$	2093.4	–
Carbon Fiber Properties			
Density	$\rho(kg/m^3)$	1790	–
Thermal Conductivity	$k(W/mK)$	6.14	–
Anisotropy of Composite	x_{k_c}	10.4 [33]	–
Specific Heat	$C_p(J/kgK)$	879.228	–
Cure Kinetics			
Enthalpy	$H_r(J/g)$	600 [16,37–39]	350–650
Activation Energy	$E_a(kJ/mol)$	600 [16,37–39]	45–80
Rate Constant	$A(1/s)$	–	–
Primary Order	n	600 [16,37–39]	–
Secondary Order	m	600 [16,37–39]	0–0.4
Diffusion coefficient	C	14.5 [4]	–
Diffusion threshold	α_c	0.9	–
Heat Transfer			
Ambient temperature	$T_{amb}(K)$	293.15	–
Heat transfer coefficient	$h_{amb}(W/m^2K)$	15	–
Surface emissivity	ε	0.97	–
Neat Epoxy Geometry			
Height	$h(cm)$	3	–
Extrusion Radius	$r_o(mm)$	0.5	–
dCF Composite Geometry			
Mass percent of dCFs	x_{dCF}	0	0–0.6
cCF Composite Geometry			
Mass percent of cCFs	x_{dCF}	0	0–0.6

References

[1] J.A. Pojman, et al., Binary frontal polymerization: a new method to produce simultaneous interpenetrating polymer networks (SINs), J. Polym. Sci. A Polym. Chem. 35 (2) (1997) 227–230, https://doi.org/10.1002/(SICI)1099-0518(19970130)35:2%3C227::AID-POLA4%3E3.0.CO;2-P.

[2] M.R. Kessler, S.R. White, Cure kinetics of the ring-opening metathesis polymerization of dicyclopentadiene, J. Polym. Sci. A Polym. Chem. 40 (14) (2002) 2373–2383, https://doi.org/10.1002/pola.10317.

[3] K.B. Manning, et al., Self assembly–assisted additive manufacturing: direct ink write 3D printing of epoxy–amine thermosets, Macromol. Mater. Eng. 304 (3) (2019) 1800511, https://doi.org/10.1002/mame.201800511.

[4] I.D. Robertson, et al., Rapid energy-efficient manufacturing of polymers and composites via frontal polymerization, Nature 557 (7704) (2018) 223–227, https://doi.org/10.1038/s41586-018-0054-x.

[5] Q. Li, et al., Advances in frontal polymerization strategy: From fundamentals to applications, Prog. Polym. Sci. 127 (2022) 101514, https://doi.org/10.1016/j.progpolymsci.2022.101514.

[6] G. Hu, et al., Rapid preparation of MWCNTS/epoxy resin nanocomposites by photoinduced frontal polymerization, Materials 13 (24) (2020) 5838, https://doi.org/10.3390/ma13245838.

[7] J.-P. Pascault, R.J. Williams, Epoxy polymers: new materials and innovations, 2009, John Wiley & Sons.

[8] S. Scognamillo, et al., Frontal cationic curing of epoxy resins in the presence of defoaming or expanding compounds, J. Appl. Polym. Sci. 131 (11) (2014), https://doi.org/10.1002/app.40339.

[9] A. Mariani, et al., UV-ignited frontal polymerization of an epoxy resin, J. Polym. Sci. A Polym. Chem. 42 (9) (2004) 2066–2072, https://doi.org/10.1002/pola.20051.

[10] M. Sangermano, et al., Photoinduced cationic frontal polymerization of epoxy–carbon fibre composites, Polym. Int. 68 (10) (2019) 1662–1665, https://doi.org/10.1002/pi.5875.

[11] M.S. Malik, et al., Review on UV-induced cationic frontal polymerization of epoxy monomers, Polymers 12 (9) (2020) 2146, https://doi.org/10.3390/polym12092146.

[12] A. Dourani, M. Haghgoo, M. Hamadanian, Multi-walled carbon nanotube and carbon nanofiber/polyacrylonitrile aerogel scaffolds for enhanced epoxy resins, Compos. B Eng. 176 (2019) 107299, https://doi.org/10.1016/j.compositesb.2019.107299.

[13] A.D. Tran, et al., Radical induced cationic frontal polymerization for preparation of epoxy composites, Compos. A Appl. Sci. Manuf. 132 (2020) 105855, https://doi.org/10.1007/s00706-020-02726-y.

[14] J.A. Pojman, V.M. Ilyashenko, A.M. Khan, Free-radical frontal polymerization: Self-propagating thermal reaction waves, J. Chem. Soc. Faraday Trans. 92 (16) (1996) 2825–2837, https://doi.org/10.1039/FT9969202825.

[15] O. Uitz, et al., Fast, low-energy additive manufacturing of isotropic parts via reactive extrusion, Addit. Manuf. 41 (2021) 101919, https://doi.org/10.1016/j.addma.2021.101919.

[16] Z. Zhang, et al., Direct writing of continuous carbon fibers/epoxy thermoset composites with high-strength and low energy-consumption, Addit. Manuf. 47 (2021), https://doi.org/10.1016/j.addma.2021.102348.

[17] C. Gao, et al., Collaborative printing and in-situ frontal curing of highly-viscous thermosetting composites, J. Manuf. Process. 89 (2023) 1–9, https://doi.org/10.1016/j.jmapro.2023.01.048.

[18] Z. Zhang, et al., Frontal polymerization-assisted 3D printing of short carbon fibers/dicyclopentadiene composites, J. Manuf. Process. 71 (2021) 753–762, https://doi.org/10.1016/j.jmapro.2021.10.014.

[19] P. Goldfeder, et al., Mathematical modeling of free-radical polymerization fronts, J. Phys. Chem. B 101 (18) (1997) 3474–3482, https://doi.org/10.1021/jp962150v.

[20] S.E. Solovyov, V.M. Ilyashenko, J.A. Pojman, *Numerical modeling of self-propagating polymerization fronts: The role of kinetics on front stability.* Chaos: An Interdisciplinary, J. Nonlinear Sci. 7 (2) (1997) 331–340, https://doi.org/10.1063/1.166248.

[21] Y. Gao, et al., Controllable frontal polymerization and spontaneous patterning enabled by phase-changing particles, Small 17 (42) (2021) e2102217.

[22] Y. Gao, et al., Anisotropic frontal polymerization in a model resin–copper composite. Chaos: An Interdisciplinary, J. Nonlinear Sci. 32 (1) (2022), https://doi.org/10.1063/5.0077552.

[23] T. Topkaya, Y. Gao, P.H. Geubelle, Frontal polymerization in short-fiber-reinforced thermoset composites, ACS Appl. Polym. Mater. 4 (10) (2022) 6880–6886, https://doi.org/10.1021/acsapm.2c00818.

[24] A. Tarafdar, et al., Three-dimensional modeling of frontal polymerization for rapid, efficient, and uniform thermoset composites manufacturing, Compos. B Eng. (2023) 111029, https://doi.org/10.1016/j.compositesb.2023.111029.

[25] E. Goli, S.R. Peterson, P.H. Geubelle, Instabilities driven by frontal polymerization in thermosetting polymers and composites, Compos. B Eng. 199 (2020), https://doi.org/10.1016/j.compositesb.2020.108306.

[26] E. Goli, et al., Frontal Polymerization of Dicyclopentadiene: A Numerical Study, J Phys Chem B 122 (16) (2018) 4583–4591, https://doi.org/10.1021/acs.jpcb.7b12316.

[27] E. Goli, T. Gai, P. Geubelle, Impact of boundary heat losses on frontal polymerization, J. Phys. Chem. B 124 (29) (2020) 6404–6411, https://doi.org/10.1021/acs.jpcb.0c03107.

[28] S. Vyas, et al., Manufacturing of unidirectional glass-fiber-reinforced composites via frontal polymerization: A numerical study, Compos. Sci. Technol. 184 (2019), https://doi.org/10.1016/j.compscitech.2019.107832.

[29] R. Auvergne, et al., Biobased thermosetting epoxy: present and future, Chem. Rev. 114 (2) (2014) 1082–1115, https://doi.org/10.1021/cr3001274.

[30] E. Frulloni, et al., Numerical modeling and experimental study of the frontal polymerization of the diglycidyl ether of bisphenol A/diethylenetriamine epoxy

system, J. Appl. Polym. Sci. 96 (5) (2005) 1756–1766, https://doi.org/10.1002/app.21644.
[31] Y. Wang, Modeling the through-thickness frontal polymerization of unidirectional carbon fiber thermoset composites: Effect of microstructures, J. Appl. Polym. Sci. 139 (31) (2022), https://doi.org/10.1002/app.52735.
[32] Z. Zhang, et al., 3D Printing of frontal-polymerized multiscale epoxy thermoset and composites, 2022. https://doi.org/10.1016/j.mfglet.2022.07.079.
[33] T. Tian, K.D. Cole, Anisotropic thermal conductivity measurement of carbon-fiber/epoxy composite materials, Int. J. Heat Mass Transf. 55 (23–24) (2012) 6530–6537, https://doi.org/10.1016/j.ijheatmasstransfer.2012.06.059.
[34] Z. Chen, et al., Multiphysics modeling of frontal polymerization-assisted layer-by-layer additive manufacturing of thermoset polymer components, Addit. Manuf. 59 (2022) 103182, https://doi.org/10.1016/j.addma.2022.103182.
[35] A. Kumar, Y. Gao, P.H. Geubelle, Analytical estimates of front velocity in the frontal polymerization of thermoset polymers and composites, J. Polym. Sci. 59 (11) (2021) 1109–1118, https://doi.org/10.1002/pol.20210155.
[36] S. Vyas, et al., Frontal vs. bulk polymerization of fiber-reinforced polymer-matrix composites, Compos. Sci. Technol. 198 (2020) 108303, https://doi.org/10.1016/j.compscitech.2020.108303.
[37] C.N. Cascaval, et al., Kinetics of the curing reaction of selected epoxy resin-amine systems, Polimery 51 (3) (2006) 199–205. https://doi.org/10.14314/polimery.2006.199.
[38] R. Hardis, et al., Cure kinetics characterization and monitoring of an epoxy resin using DSC, Raman spectroscopy, and DEA, Compos. A Appl. Sci. Manuf. 49 (2013) 100–108, https://doi.org/10.1016/j.compositesa.2013.01.021.
[39] R.D. Patel, R.G. Patel, V.S. Patel, Effect of the anhydride structure and the epoxy fortifier on the reactivity in curing of epoxy resins, Die Angewandte Makromolekulare Chemie: Applied Macromolecular Chemistry and Physics 155 (1) (1987) 57–66, https://doi.org/10.1002/apmc.1987.051550105.